Remote and proximal sensing for sustainable water use in almond orchards in southeast Spain in a digital farming context.

Á. Sánchez-Virosta[1], D. Gómez-Candón[1], F. Montoya[2], Y. Pérez[1], V. Jiménez[2], J. González-Piqueras[1], R. López-Urrea[3], J.M. Sánchez[1]

[1]University of Castilla-La Mancha, Regional Development Institute, Albacete, Spain.
[2]Instituto Técnico Agronómico Provincial de Albacete and FUNDESCAM, Albacete, Spain
[3]Desertification Research Centre (CIDE), CSIC-UV-GVA, Valencia, Spain

Abstract.

Agriculture, particularly in arid and semi-arid regions, consumes a significant portion of global water resources, necessitating precise and cost-effective monitoring techniques for crop water status to enhance water use efficiency and crop productivity.. This scenario of water scarcity, underscores the need for a more effective and precise monitoring of the crop water status to optimize irrigation scheduling and improve crop water use efficiency. Remote and proximal sensing, combining visible, multispectral and thermal capabilities at different scales allows to estimate water needs, detect and quantify crop water stress, or identify different productivity zones within an orchard.

The research demonstrates that the Crop Water Stress Index (CWSI), derived from both ground-based UAS-based monitoring, is a reliable indicator of water status in almond. This study highlights the successful correlation of CWSI with physiological traits stomatal conductance (gs), net carbon assimilation (An) and, especially with stem water potential ($R^2 \geq 0.85$). In general, the results obtained underscore the utility of UAS in almond precision agriculture. CWSI was able to detect water stress before water deficit was enough to impact net carbon assimilation, providing timely data for operational water management. The integration of CWSI with multispectral vegetation indices (VIs) from UAS further extends its applicability, offering a practical and effective solution for large-scale monitoring. The study explores 34 multispectral vegetation indices (VIs), highlighting the results of those pigment-related ones such as the Canopy Chlorophyll Content Index (CCCI),, the MERIS Terrestrial Chlorophyll Index (MTCI), the Carotenoid Reflectance Index 2 (CRI2), and the Anthocyanin Reflectance Index 2 (ARI2) and their relationship with ground-based physiological measurements. These indices offer a validated approach for detailed physiological monitoring, enhancing decision-making related to almond crop management. Besides, the creation of Growth Variability Maps (GVMs) from satellite data, integrated with UAS-based CWSI maps, further refines the monitoring process, enabling targeted water application and optimizing resource use. UAS-based CWSI provided high-resolution spatial data, capturing the variability of water stress and cumulated transpiration across the orchards. The findings also emphasize the need for meticulous data pre-treatment and calibration in thermal monitoring to achieve reliable results.

This comprehensive approach provides a robust framework for improving water use efficiency in almond orchards, particularly in water-scarce regions like southeast Spain.In conclusion, the study confirms the practicality and effectiveness of UAS-based thermal imaging and multispectral analysis for real-time water stress monitoring in almonds, offering significant implications for enhancing agricultural water management practices.

Keywords.
Evapotranspiration, UAS, thermal remote sensing, water stress, canopy temperature.

Introduction

Considering the evolving climate change and the increasing disparity between water availability and demand, agricultural producers face significant water resource constrains, particularly in arid and semi-arid regions (Martínez-Valderrama et al. 2023; Tian et al. 2023). Currently, agricultural activities account for a substantial portion—ranging from 70% to 90%—of global water utilization (Morison et al. 2007). Consequently, there is an imperative to enhance agricultural water use efficiency through improved irrigation practices and the implementation of precise, cost-effective, and timely monitoring protocols for assessing crop water status. Aiming to augment both the quantity and profitability of food production while conserving water resources, the identification and measurement of plant stresses are of considerable importance for agriculture as a whole and for precision farming specifically (Neupane and Guo 2019). A paradigmatic case in this context is the cultivation of almond trees (*Prunus dulcis (Mill.) D.A. Webb*). The harvested area of this crop have increased in more than 350% globally during the last 70 years (FAOSTAT data, 2023). Specifically in Spain, the irrigated almond tree extension has doubled between 2015 and 2022 (MAPA, 2022), especially in water-scarce regions, such as those of southeast Spain. In this context, the need for better and more accurate monitoring of almond trees water status is crucial for their future profitability in the medium term.

Water stress monitoring can rely on direct measurements of soil water content and crop physiological traits on-site, such as stomatal conductance, net carbon assimilation or water potential. Despite its demonstrated accuracy and reliability, these methos are characterized by considerable time investment, labor requirements, and financial costs (Joaquim Miguel Costa et al. 2019). Moreover, such methods often fail to address the spatial heterogeneity inherent in soil and crop distribution. Alternatively, remote sensing techniques offer distinct advantages, notably through assessments of canopy temperature or canopy reflectance, owing to their ease of implementation, non-invasiveness, and reduced labor demands (Araus and Cairns 2014). Remote sensing stands out as a potential tool, facilitating spatiotemporal monitoring of water stress and irrigation management(Bhatti et al. 2023).

At present, numerous studies are conducted on crop water stress assessment using satellite data (Ahmad et al. 2021; Campoy et al. 2019). However, an operational and easy-to-use crop monitoring often require high temporal frequency and sufficiently detailed spatial resolution to detect water deficit. The detection of early water deficit, for example by initial stages of declined stomatal conductance or water potential allows for effective data-driven decision-making. In this regard, satellite remote sensing products are limited by relatively low spatial-temporal resolution and susceptibility to weather conditions (e.g. clouds). Additionally, in woody crops, such as almonds, where the vegetation cover does not encompass the entire image, further complicates the interpretation of satellite-derived results. Conversely, UAS-based remote sensing offers high flexibility, short operational cycle, and high resolution, reaching very precise levels of detail for an effective decision-making on crop water stress assessment at farm level (Burchard-Levine et al. 2024). Numerous indices derived from drone imagery, including multispectral, thermal, and even RGB-based images, have studied water stress monitoring in crops.

Thermal indices are commonly used for evaluating crop water status (Costa et al. 2019; Sánchez-Virosta and Sánchez-Gómez 2020). This is based on the principle that crop canopy temperature (Tc) rises with increasing water deficit. An early response to water deficit in plants is stomatal closure, which reduces transpiration and a decline in evaporative cooling, and thus raises leaf and canopy temperatures. Many studies have integrated thermal cameras on UAS platforms to assess water stress in several crops, especially in herbaceous (Gómez-Candón et al. 2021) but also in woody crops (Gómez-Candón et al. 2016). Some attempts have been carried out on UAS-based thermal monitoring in almond (Guimarães et al. 2024 and references therein). However, Tc data should be carefully monitored. Tc is influenced not only by water supply but also by micrometeorological conditions such as air temperature (Ta), relative humidity (RH), and vapor pressure deficit (VPD). To buffer this meteorological effect on Tc, the Crop Water Stress Index (CWSI,Idso et al. 1981) based on canopy temperature and certain meteorological parameters, has been investigated as an effective method for monitoring the water status of woody species

Proceedings of the 16th International Conference on Precision Agriculture
21-24 July, 2024, Manhattan, Kansas, United States

2

like grapevines (Prueger et al. 2019), peaches(Joaquim Bellvert et al. 2016; Ramírez-Cuesta et al. 2022), olives (Berni et al. 2009; Roma et al. 2023), and also in almond (Joaquim Bellvert et al. 2018; Gonzalez-Dugo et al. 2019; Gutiérrez-Gordillo et al. 2020). These studies generally report promising results on CWSI as a tool for water stress monitoring. However, it is also well-recognized that UAS-based thermal data also have constraints. For example, Gutiérrez-Gordillo et al. (2020) tried UAS-based CWSI monitoring which was not precise enough to capture the differences between control and deficit-irrigated trees that were observed with stem water potential. In this, sense unstable canopy temperature acquisition and low mosaic precision, necessitates complex pre-treatments like radiometric calibration, temperature correction, and canopy temperature extraction. Therefore, pre-treatment and thermal calibration, along with comparison and correction of this data with ground-based infrared thermometry is crucial for its reliability as an operative tool. Along with this, to corroborate CWSI utility as a management tool more studies are needed to address the correlations between CWSI with physiological traits and its capability to detect intra-plot variability. Hence, this study tries to address these factors, being essential for the assessment of CWSI as a potential tool for decision-making in almond irrigation management.

In addition, multispectral vegetation indices (VIs), which result from mathematical operations on vegetation reflectivity, can be used to monitor the condition of surface vegetation. VIs have been successfully applied in agronomy on diseases detection, physiological performance, and water deficit monitoring (Ali et al. 2019; Berger et al. 2022; Sishodia et al. 2020). In this sense, water stress can affect the structure of the vegetation canopy, photosynthesis, and leaf moisture content. In this study, we calculated up to 34 VIs from a multispectral sensor and compared them not only with CWSI obtained from thermal flights but also with ground-based physiological measurements to assess multispectral UAS-based data as a potential tool for precision agricultural management.

Finally, despite management practices within agricultural plots are typically uniform over time and space for a single crop, characterizing intra-field variability is crucial for sustainability and resource efficiency. UAS-based monitoring along with satellite data and ground proximal sensing enable precise determination of growth differences and water needs aiding agronomic decision-making. Growth Variability Maps (GVMs) from satellite imagery, effectively describe variability and inform management decisions. This study addresses the validation GVMs' ability to identify intra-field growth differences in almond trees, using high-resolution drone data and distributed plot measurements, providing insights into the causes of variability within farm level.

The primary objective of this study is to evaluate and analyze UAS-based data as innovative and operational tools for detecting water deficit in almond trees. Additionally, the study aims to assess the variability within almond plots and evaluate how thermal and multispectral data correlate with ground-based physiological variables in almonds. This will open a window for the identification of limitations and potential improvements on decision-making tools from UAS-based measurements in almond orchards.

Material and Methods

Field sites and experimental design
Two commercial drip-irrigated almond orchards situated within the Albacete province (SE Spain) were subject to monitoring, each positioned approximately 25 km apart. The first study site, situated in Hellín (38.48417N, -1,78583W), with 12.5 hectares (cv. Penta) was established in 2018, with a plantation framework of 6 m x 5 m. As depicted in Figure 1, the experimental design in Hellín incorporates complete random blocks, encompassing three distinct irrigation treatments, non-deficit (ND), moderate deficit (MD) and severe deficit (SD). Each irrigation treatment was replicated in three plots, comprising each plot 15 trees, arranged in three rows of five plants each. A daily irrigation based on the soil's water balance without any water restriction was applied in the ND treatment. The dual crop coefficient (Kcb + Ke), as proposed by Allen et al. (1998) and recently updated by Rallo et al. (2021), was applied. Thus, four different stages (I, II, III and IV)

Proceedings of the 16th International Conference on Precision Agriculture
21-24 July, 2024, Manhattan, Kansas, United States

3

were defined as follow: stage I: from swollen bud to onset of fruit set; stage II: from onset of fruit set to fruit final size; stage III: from fruit final size to harvest; and stage IV: from harvest to onset of leaf drop. ND treatment was designed to receive the 100% of the crop water requirements (CWR) across the four former stages; MD wasdesigned as ND but receiving the 75% of the CWR during the stage III; while SD, was designed to receive the following percentages of the CWR: 100% during the stage I, 75% during stages II and IV, and 50% during stage III. Due to a delay in the installation of the irrigation system, the contribution in percentage of total irrigation with respect to the ND was 22% less for the SD treatment and 7% less for the MD treatment (Fig.2B).

The other site, in Tarazona de la Mancha (Tzn) (39.2660N, -1.9397W) the almond orchard with 10 ha, was established in 2017. In this instance, plant and row spacings was 4.5 and 6.5 m respectively, resulting in a density of 342 trees per hectare (Fig. 1). Identical units of N-P-K as those applied in Hellín were applied, adhering to the recommended fertilization program. Irrigation was based on farmer decision, with lower frequencies of irrigation but in higher amount of water per irrigation event compared to Hellín (Fig. 2A).
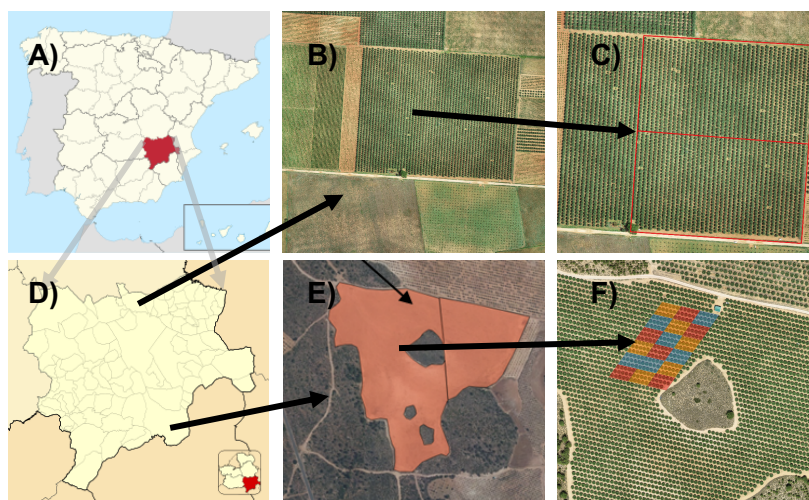

Figure 1. Location of the two almond orchards within Spain 3A) and 3D) the province of Albacete. In 3B) an aerial image of the Tarazona plot is provided with irrigation sectors marked in red in 3C). The almond orchard of Hellín highlighted in orange in 3E) is divided in 3F) three different irrigation treatments: red is severe deficit; orange is mild deficit and blue is control (no deficit applied).

Meterological data measurements

Both almond orchards are provided with a full-equipped weather station. In Hellín, meteorological instruments are placed in a mast at a height of 5.0 m above the ground, whereas in TzM the instrumentation was deployed in a tower at a height of 6 m, to guaranty 2 m separation from the canopy top. Data were recorded at 15-minute, hourly, and daily intervals using CR1000 and CR1000X dataloggers (Campbell Scientific Instrument, Logan, UT, USA). The variables measured included the four components of the net radiation (models CNR01 in Hellín and, NR01, Hukseflux, Delft, The Netherlands), air temperature and relative humidity (HC2A-S3, Campbell Scientific Instrument, Logan, UT, USA in Hellín, and HMP45AC, Vaisala, Helsinki, Finland in TzM), wind speed and direction (03002 Wind Sentry, R.M. Young, Traverse City, MI, USA), and rainfall (52203 Rain Gauge, R.M. Young, Traverse City, MI, USA).

Two sets of 4 thermal InfraRed thermometers (IRT) each (SI-121 and SI-421, Apogee Instruments, Inc., Logan, UT, USA) were deployed in both orchards for the continuous thermal monitoring of the almond tree canopy and soil (Montoya et al. 2022). Three of the IRTs were assembled pointing downward with an angle of 45°, two of them to the canopy top at both, east and west side trees in Hellín, and north and south side trees in TzM, and a third to the inter-row soil. The full set of thermal measurements was completed with an additional IRT pointing upward to measure the downwelling sky radiance required for the atmospheric correction of all the radiometric temperatures. Vapour pressure deficit (VPD), utilized in the Non-Water Stress

Proceedings of the 16th International Conference on Precision Agriculture
21-24 July, 2024, Manhattan, Kansas, United States

4

Baseline (NWSB) calculation (explained in detail below), was obtained using Equation (1):

$$VPD = es \times \frac{100-RH}{100} \text{ and } es \text{ is calculated as: } es = 6.11 \times \exp(\frac{L}{Rv}(\frac{1}{273})-\frac{1}{T})) \tag{1}$$

where es is the saturation vapour pressure in mbar, L is the latent heat of vaporization (2.5 106 J kg^{-1}), Rv is the specific gas constant for water vapour (461 J K^{-1} kg^{-1}) and T is the current air temperature (K). RH is the relative humidity (%).
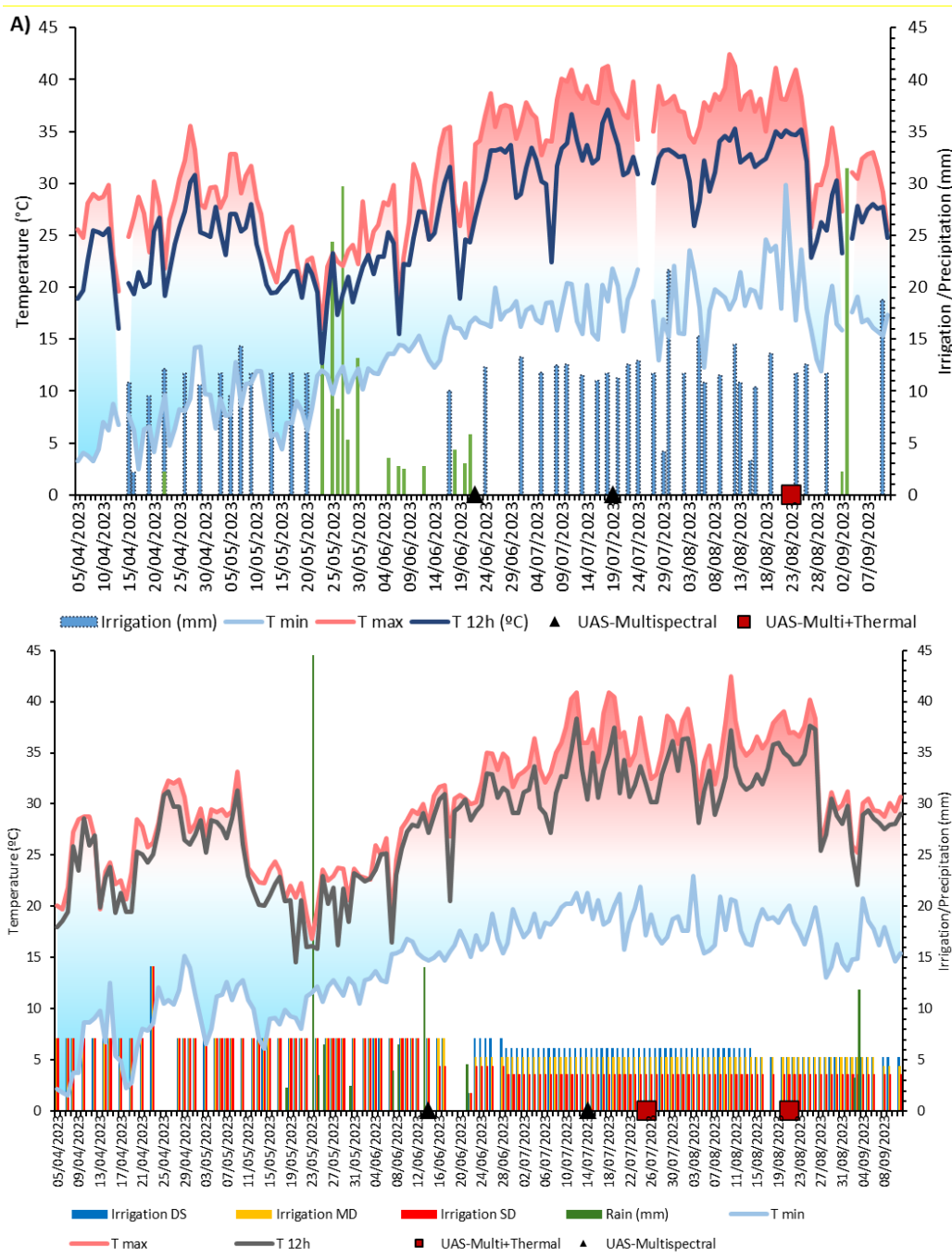

Figure 2. Evolution of air temperatures (daily minimum, daily maximum and at 12h UTC), effective precipitation and irrigation in A) Tarazona and B) Hellín. UAS flight dates are marked within the plot for each location.

Proceedings of the 16th International Conference on Precision Agriculture
21-24 July, 2024, Manhattan, Kansas, United States

5

Physiological-based and ground data collection

Gas exchange data

In Hellín site, net assimilation rate (An), stomatal conductance (gs), leaf transpiration (Emm) and internal CO^2 (Ci) values were assessed using a portable photosynthesis system for gas exchange measurements (LI6800-TX model, LI-COR Bioscience, NE, USA). The intrinsic water-use efficiency (WUEi) was computed for each plant as the ratio of An and gs. Leaf chamber parameters for data collection were adjusted based on the test area's conditions: atmospheric CO_2 concentration set at 400 µmol mol^{-1}, air temperature maintained at 25.0 ± 0.5 ºC, relative humidity at 70 ± 5 %, airflow set at 650 µmol s^{-1}, and photosynthetic photon flux density (PPFD) at 1500 µmol m^{-2} s^{-1}. Concurrently with UAS multispectral and thermal flights, gas exchange readings were taken in the two central trees of each plot within the three treatments.

High accuracy infrared thermal data

Concurrent to each UAS flight time, temperature transect measurements were performed with a CIMEL Electronique CE 312-2 high-accuracy multispectral thermal radiometer (Legrand et al. 2000). This instrument has five narrow bands and a broadband in the spectral range between 8 and 13 µm. For this work channel 3 (10.2-11.0 µm) was selected for the measurements (Coll et al. 2019). Specifically, three almond trees per irrigation treatment were monitored, covering East, South, West and North orientations of the trees. Radiometric temperatures, both from CIMEL and IRT were atmospheric corrected from downwelling sky radiance and almond canopy emissivity effects following the procedure described in Sánchez et al. (2014).

Stem water potential

Almond stem water potential (SWP, MPa) was evaluated concurrent to each UAS flight between May and September in both locations. In Hellín, a total of 12 SWP measurements per treatment were conducted, measuring 2 central trees within each of the 6 plots per treatment, resulting in a total of 36 measurements. In Tzn, 4 different areas within the orchard were selected for SWP monitoring based on the growth variability maps of the previous season. In those areas, 3 trees were measured. All the SWP were performed using the same Scholander pressure chamber (PMS Instruments; Corvallis, OR, USA). For sampling, one shaded leaf per tree near the trunk base (two trees per elementary plot) were selected, with the chosen leaves covered in aluminum foil for at least one hour before measurement.

UAS flights

For the acquisition of thermal data, a Zenmuse H20T camera (Zenmuse XT, FLIR System, Inc., USA, 8-14 µm) with a resolution of 640 × 512 pixels and a 24 mm focal length, with a FOV of 40.6° was mounted on a DJI Matrice 350 RTK UAS. An altitude of ~80 m was set for the flight plans, providing a Ground Sample Distance (GSD) of 10 cm. The thermal imagery was calibrated using ground temperature data collected with an Apogee MI-220 radiometer on ground temperature measurements. The same UAS platform was employed for multispectral flights using the MicaSense RedEdge P sensor (Micasense, 1300N NorthlakeWay, Seattle, USA), provided with five spectral bands located at the wavelengths 475 ± 32 nm (blue), 560 ± 27 nm (green), 668 ± 14 nm (red), 717 ± 12 nm (red edge), and 842 ± 57 nm (near infrared), and a field of view (FOV) of 50°, achieving a GSD of 5 cm in this case. Flights were conducted from May to September of 2023, centered at ~12:00 h GMT, always under clear-sky conditions and with a wind speed below 12 m/s. The thermal infrared and multispectral mosaic images were acquired using the photogrammetric PIX4Dmapper© sofware.

CWSI calculation and CWSI maps

Canopy temperatures obtained from both, ground measurements using the CIMEL and H20T thermal images from UAS flights, were used to estimate the Crop Water Stress Index (CWSI). For this purpose, the following equation was used:

Proceedings of the 16th International Conference on Precision Agriculture
21-24 July, 2024, Manhattan, Kansas, United States

6

$$CWSI = \frac{(\text{Tc}-\text{Ta})-(Tc-Ta)LL}{(\text{Tc}-\text{Ta})\text{UL}-(Tc-Ta)LL} \qquad (2)$$

where (Tc-Ta) represents the measured difference between canopy and air temperatures; (Tc-Ta)LL is the expected lower limit of this difference for a potentially transpiring canopy, and (Tc-Ta)UL represents the expected differential for a non-transpiring canopy. The lower and upper limits of *equation (2)* can be derived following the methodology proposed by Idso et al. (1981). Under optimal water availability conditions, Tc-Ta exhibits a linear relationship with the vapor pressure deficit (VPD), forming the Non-Water-Stressed Baseline (NWSB). The upper limit is a constant, obtained from the highest Tc-Ta values of the dataset. This method is contingent on the climatic conditions of the site. The NWSB establishes the lower limit for calculating the Crop Water Stress Index (CWSI) and can be empirically determined by regressing the canopy-air temperature differential (Tc-Ta) against the VPD on clear, sunny days under optimal irrigation conditions, typically measured around midday. The dataset utilized to calculate the NWSB, was obtained from both sites in Tarazona and Hellín (outside the irrigation treatment plots), in those days under optimal irrigation conditions to collect a comprehensive dataset from May to August 2023 with values assessed at 15-minute intervals between 10:00 and 12:00 UTC. The UAS-based temperature data were used to estimate CWSI maps.

CWSI maps

To generate orthomosaics and vectorize tree crowns, images were acquired from a DJI Phantom 4 RTK drone. These images were subsequently processed to create precise orthomosaics, Digital Surface Models (DSMs), and Digital Terrain Models (DTMs). All captured data were converted into accurate geospatial information using PIX4Dmapper© sofware, version 4.6.4 (PIX4D S.A., Prilly, Switzerland). Each type of sensor produced specific raster layers that were calibrated and aligned to ensure consistency among the various data sources. Subsequent data processing was conducted in QGIS software, version 3.28.10 (QGIS Development Team, Open Source Geospatial Fundation Project). To discriminate tree crowns from the underlying soil, the difference between the DSM and DTM was calculated. A geospatial grid, aligned with the tree planting pattern, was designed, with each grid element corresponding to an individual tree and assigned a unique ID.

Growth Variability Maps

The Growth Varibility Maps were developed based on the determination of daily potential transpiration. Using the Kcb/NDVI relationship proposed by Campos et al. (2010):

$K_{cb}=1.44 \cdot NDVI - 0.1$ (3)

where we obtain the basal crop coefficient (K_{cb}). This coefficient, together with daily data of the grass reference evapotranspiration (ET_o) and NDVI (obtained from the temporal interpolation of NDVI values derived from satellite images), allows the derivation of sequences for the accumulated potential transpiration. The TONIpbp, an own developed model, operates pixel by pixel, within the specified time interval from the start to the end of the desired crop cycle. The result is a map of accumulated potential transpiration for the specified area. Equation 4 synthesizes the growth model that allows the calculation of accumulated potential transpiration:

$$T_{p,acum} = \int_{t_0}^{t} T_p \cdot d(t) = \int_{t_0}^{t} K_{cb} \cdot ET_o \cdot d(t) \qquad (4)$$

where $Tp,acum$ is the potential transpiration per unit area accumulated during the period between t_0 and t_t in mm; Tp is the potential transpiration of the crop in mm; K_{cb} is the basal crop coefficient (dimensionless); ETo is the grass reference evapotranspiration in mm·day^{-1}, obtained from the nearest meteorological station.

For each spatial unit, in this case, the satellite pixel size, the variable T can vary due to various factors both biotic and abiotic. Therefore, based on the accumulated potential transpiration during the entire growth cycle of a crop in a given pixel along with the average accumulated potential transpiration value of the plot, variability can be calculated as:

Proceedings of the 16th International Conference on Precision Agriculture
21-24 July, 2024, Manhattan, Kansas, United States

7

$$\text{Variability} = \frac{T_{p,acum}}{\overline{T}_{p,acum}} \hspace{6cm} (5)$$

where $Tp,acum$ is the accumulated potential transpiration value during the entire growth cycle of the crop in a given pixel, in mm; $\overline{T}_{p,acum}$ is the average accumulated potential transpiration value of the plot, in mm.

Statistical analysis

ANOVA analyses were performed to detect statistical differences among different factors (irrigation treatment or site) for CWSI and VIs data. Pearson correlations and test for the significance of the regression coefficients were also conducted for the parametrization of CWSI, Vis and physiological data. All the statistical analyses were done using RStudio (R version 4.3.3).

Results and Discussion

Non-Water Stress Baseline (NWSB)
Unlike the traditional method, which utilizes dry and wet references, the NWSB in the empirical approach is established by relating Tc-Ta to vapor pressure deficit (VPD) through linear regression analysis. This empirical method of calculating CWSI offers the advantage of simplicity in computation, requiring only two additional parameters (air temperature and relative humidity). Idso et al., (1981) reported that different crops had their own unique NWSBs. However, even for the same crop, NWSB can change being dependent on factors such as seasonal or hourly differences (Romero-Trigueros et al. 2019; Sánchez-Piñero et al. 2022), crop phenological stage (Zhang et al. 2019), or cultivar(Gutiérrez-Gordillo et al. 2020) among others factors. This sensitivity of the empirical NWSB to changes in location and climate variables has been a subject of criticism in some studies (Gonzalez-Dugo et al. 2014; Gonzalez-Dugo and Zarco-Tejada 2024).
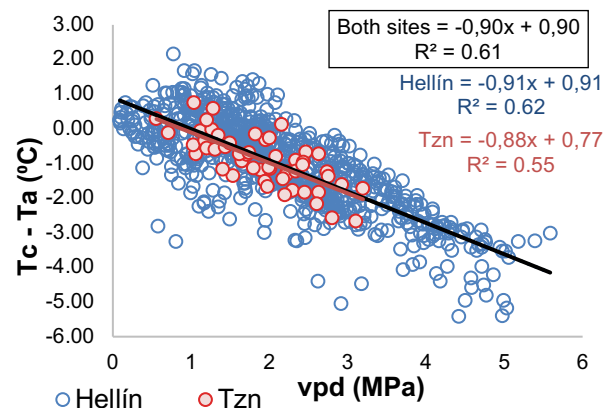

Figure 3. NWSB of the CWSI at the distinct locations. Blue dots correspond to Hellín and red dots to Tarazona. Different equations and R2 are obtained depending on the source of data: Equation in blue corresponds to data in Hellín, in red in Tzn and in black is the consolidated one with data from the two plots.

However, in the present study, a remarkable alignment was observed between the two locations, Tzn and Hellín, where the slopes of the NWSB were -0.91 and -0.88, respectively. In Tzn dataset, fewer data points are shown due to both unfavorable weather conditions or longer periods of irrigation restrictions, as shown in Fig. 2A. However, this dataset presented similar slope that the one obtained in Hellín, allowing to consolidate the same NWSB for both locations obtaining a slope of -0.90. These specific-location slopes and the consolidate one, are in agreement with those found onBellvert et al. (2016). Despite criticisms surrounding the empirical NWSB model's sensitivity to location-specific and climate-related factors, this study demonstrates a notable alignment between two distinct locations. This good alignment found here could be related to a proper instrument calibration and atmospheric correction along with the regular calibration of the used thermal sensors with high accuracy black bodies. Besides, the elimination of data points when climatic parameters or irrigation supply were not ideal was carefully assessed. In this sense,

**Proceedings of the 16th International Conference on Precision Agriculture
21-24 July, 2024, Manhattan, Kansas, United States**

8

these factors are essential in thermal monitoring and sometimes are overlooked (Tunca et al. 2023). By achieving this consolidation on the NWSB for both locations, the study reaches an operational efficiency in almond CWSI calculations. Nevertheless, these NWSBs results need to be corroborated in future studies to corroborate this promising results.

Ground and UAS-based CWSI of almond and its correlation with physiological variables
The empirical CWSI results, despite its relatively stable range (0–1) for quantifying crop water stress, may also be sensor-, site- and climate-specific, or could vary annually due to differences in micro-meteorological conditions within the same field. To corroborate the reliability of CWSI measurements, an analysis of the correlations between CWSI derived from both ground-based measurements (CWSI_CIMEL in Fig. 4) and that obtained from UAS measurements (CWSI_UAS, in Fig. 5) were carried out.
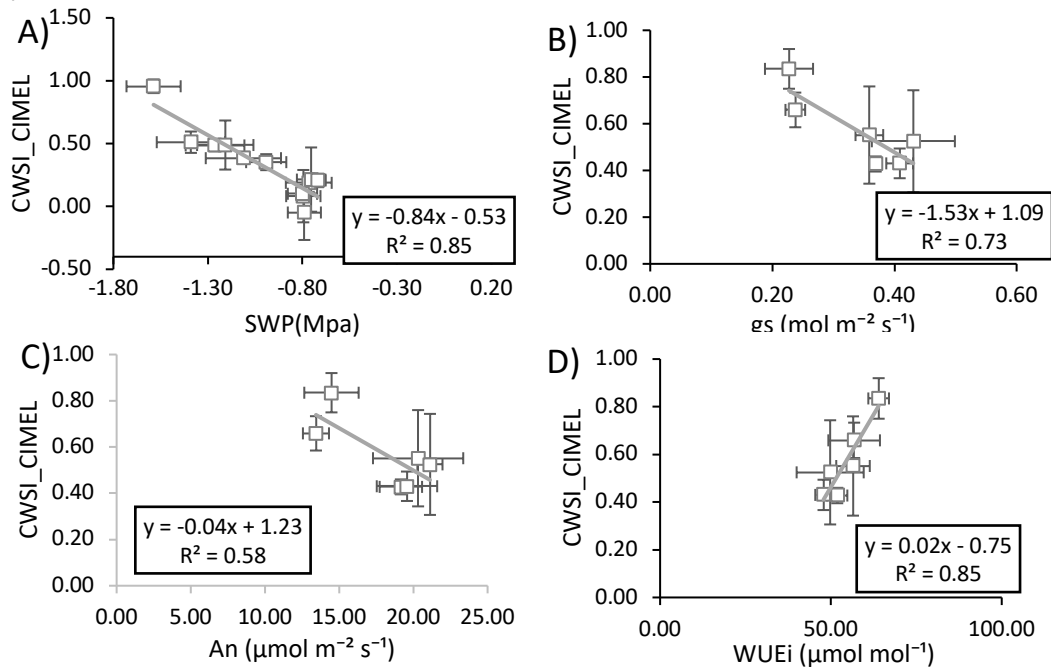

Figure 4. Relationships between CWSI obtained with a CIMEL CE312-C2 high-precision thermal radiometer (CWSI_CIMEL) on West Canopy Orientation and A) stem water potential (SWP); B) Stomatal conductance (gs); C) Net carbon assimilation rate and D) Intrinsic Water Use Efficiency (WUEi). Data represents mean values pooled by date and irrigation treatment in Hellín almond orchard. Error bars are standard deviation of both CWSI and physiological traits. Data was obtained in 2-3 trees randomly located in the central part of the plot and within treatments.

As depicted in Figure 4, significant correlations were found between the CWSI_CIMEL and various physiological variables. Each of these correlations was statistically significant ($p<0.05$). The most pronounced correlations were observed with SWP and WUEi, while the correlation with An was comparatively weaker. Fig. 4C, presents evidence that the variability in An was minimal, with only two values falling below 15µmol m^{-2} s^{-1}, denoting a low impact on almond photosynthesis (Sperling et al. 2023). Conversely, a higher degree of variability was noted in the remaining variables, particularly SWP. This phenomenon of increased variability in water-related traits such as SWP, gs, or WUEi compared to An is a well-documented physiological response to early water deficit, since under moderate water deficit, plants are capable of regulating water loss through stomatal closure without significantly impacting net assimilation (Chaves et al. 2003; Pardo et al. 2022).

However, it should be noted that not all CIMEL measurements performed equal and were orientation dependent. In Fig. 4 the results shown corresponds to those Tc measured at west orientation of the canopy, presenting similar results at those on N orientation, where SWP and gas exchange measurements were done. On these orientations, all the leaves were under the same conditions of shading. In contrast in South and East orientations, the R^2 of correlations with SWP decreased ca. 35%. These results emphasize the importance of protocol canopy temperature (Tc) measurements. In summary, when done properly, these thermal measurements

Proceedings of the 16th International Conference on Precision Agriculture
21-24 July, 2024, Manhattan, Kansas, United States

9

along with physiological monitoring by gas-exchange and SWP monitoring where capable to reflect the plants' water status conditions. However, these ground-based methods are labor-intensive, costly, and impractical for large-scale monitoring due to the spatial heterogeneity of water stress within agricultural fields. The UAS-based methodology tries to resolve these constrains of ground-based monitoring. In this sense, the results of CWSI (CWSI_UAS) indicate that this method can be an effective tool to detect not only physiological performance (Fig. 5) but also inner spatial variability of water stress across the orchard (see Fig. 7).
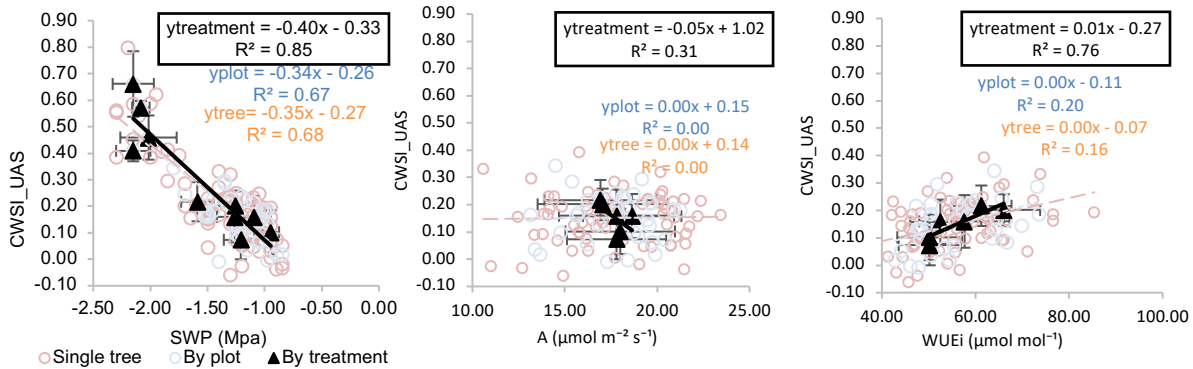

Figure 5. Relationships between CWSI and A) stem water potential (SWP); B) Intrinsic Water Use Efficiency (WUEi) and C) net carbon assimilation rate measured on August 23 in Tzn and August 21 in Hellín. Black triangles with error bars represent mean treatment values ± standard deviation. Blue dots represent plot values (2-3 trees randomly located across the plot and within treatments) and orange dots represent single tree values

As occurred with CWSI_CIMEL, strong correlations between CWSI_UAS and SWP (Fig. 5A) were found, but not only when values where aggregated by treatments and locations but also when analyzed at the plot level or even among individual trees (Fig. 5A). This result highlights the accuracy of CWSI_UAS to monitor water status even at a plant/tree scale. In this sense, Gonzalez-Dugo et al. (2019) also presented similar results in almond, suggesting that CWSI measured by UAS can be a feasible alternative to monitor water status in almond orchards. The weakest correlation was found again with net assimilation rate (An). As mentioned before, this can be an effect of water deficit affecting transpiration and leaf moisture without significantly impacting photosynthetic potential (Fig. 5B). The correlation with WUEi was also high, but only when the data was pooled by treatments and dates, obtaining weak correlations at plot or tree level. However, it can be deducted that in those treatments where more pronounced water deficit increased CWSI, stomatal closure decreased transpiration without compromising photosynthesis triggering a higher WUEi (Fig. 5C).

It should be noted that CWSI was developed as a thermal based stress indicator in herbaceous crops. In this sense, woody crops monitoring by UAS present important challenges (Sirera et al. 2021 and references therein). Unstable canopy temperature acquisition, low mosaic precision, or soil interference on Tc data are issues that need to be assessed. For this, radiometric calibration and temperature correction is crucial to improve the accuracy of CWSI measurements. In this study, the discrimination of tree crowns from the underlying soil, the radiometric calibration and temperature correction has been carefully carried out, reaching high correlation between UAS-based CWSI with stem water potential.

CWSI and Growth Varibility Maps

The CWSI maps, generated from UAS thermal sensor, effectively captured the spatial variability in water stress within the orchards as can be observed in Fig. 7. These maps, revealed distinct patterns of water stress, aligning closely with the GVM. In Tzn orchard it can be observed how, despite the whole orchard was managed in a similar way, lower CWSI values were found in the central part of the plot (Fig. 7A), coinciding with the highest values of cumulated transpiration in the GVP (Fig. 7B). In Hellín, at the date of the thermal flight, there was higher soil moisture and low CWSI values (Fig. 7C) than that observed in Tzn. This is attributed to more recent irrigation event in the flight date (Fig. 2B). However, deaspite the lowere range of CWSI values in Hellín, it

**Proceedings of the 16th International Conference on Precision Agriculture
21-24 July, 2024, Manhattan, Kansas, United States**

10

can be observed that this variability is also aligned with that presented in the GVP variability values (Fig. 7D), with the highest CWSI values and the lowest cumulated transpiration values in the southeast (values in red) of the plot. The opposite occurs in the northwest (values in blue). In Hellín, some values of CWSI were below 0. This was caused by a waterlogging effect in the northwest zone. The analysis of these images taken with the drone and the thermal sensor allowed to detect this failure. In any case, this part of the plot was not included in the ground-based measurements so it did not affect the development of correlationes previously mentioned in the study. All these results underscore the utility of CWSI maps in identifying areas within orchards that experience varying degrees of water stress or irrigation system faliures, finding inner variability due to several factors. Such spatial variability under presumably similar management condition is critical for precision irrigation management, enabling targeted water application to optimize resource use and improve crop yields.
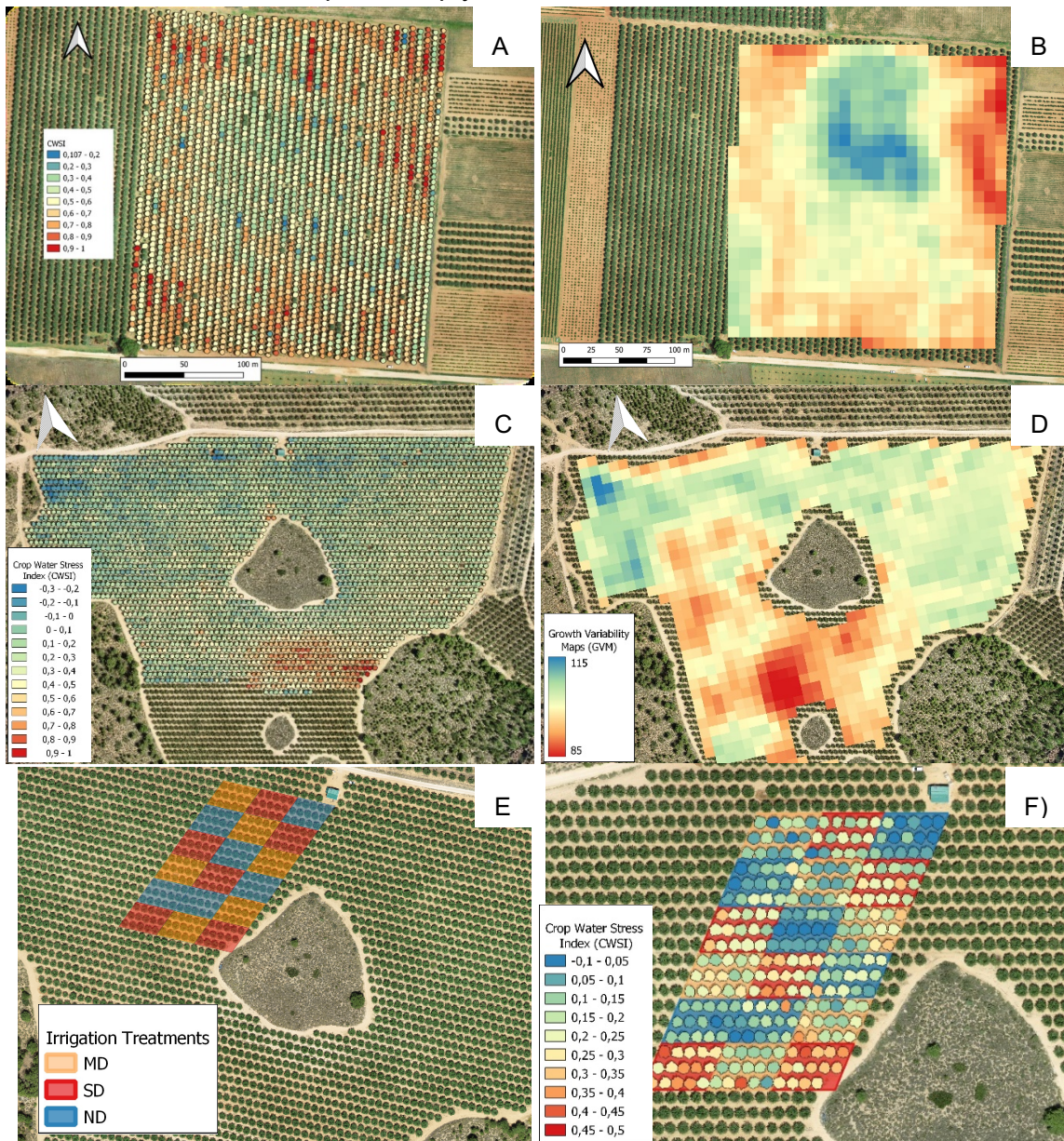

Figure 7. A) CWSI map of Tarazona almond orchard on August 23, 2023; B) Growth Variability Maps (GVM) of Tarazona plot in 2023; C) CWSI map of Hellín almond orchard on August 21, 2023 D) GVM of Hellín plot in 2023; E)Spatial distribution of the irirgation treatment assay in Hellín and E) CWSI map within the assay. CWSI was calculated using data obtained from the H20T thermal sensor mounted on a DJI Matrice 350 RTK UAS. GVM represent the variability (%) on cumulated transpiration at each pixel compared with the average transpiration in the whole plot. Data to create GVM was obtained at each location from Sentinel-2 images and reference Et$_o$.

**Proceedings of the 16th International Conference on Precision Agriculture
21-24 July, 2024, Manhattan, Kansas, United States**

11

In fact, CWSI maps were fine enough to detect variability in the different irrigation treatments plots in Hellín, even when they did not reach high stress values. In Fig. 7D it can be seen how, although no value exceeded the CWSI greater than 0.5, there is a clear trend towards lower CWSI values in those plots without deficit (marked in the blue boxes) and higher values in plots with moderate deficit (orange boxes) or severe deficit (red box). The findings of this study on CWSI maps are consistent with previous research that has utilized CWSI for assessing spatial variability in crop water stress. For example, Bellvert et al. (2014) in vineyard or Zhang et al. (2019) in maize characterized the spatial variability in water status across using CWSI maps derived from UAS thermal imagery. Their results indicated that CWSI maps were effective in assessing spatial water stress variability, similar to the outcomes observed in the current study. The application of CWSI in almond orchards presented in this study, extends the use of this index beyond other crops, showcasing its versatility across different crop types and environmental conditions.

Correlations between VIs and CWSI with ground-based measurements and CWSI_UAS

The analysis of the correlations obtained between various vegetation indices (VIs) with CWSI_UAS and ground-based physiological variables denote a high variability on the accuracy of VIs to detect water status and physiological performance on almond orchards (Fig. 8).
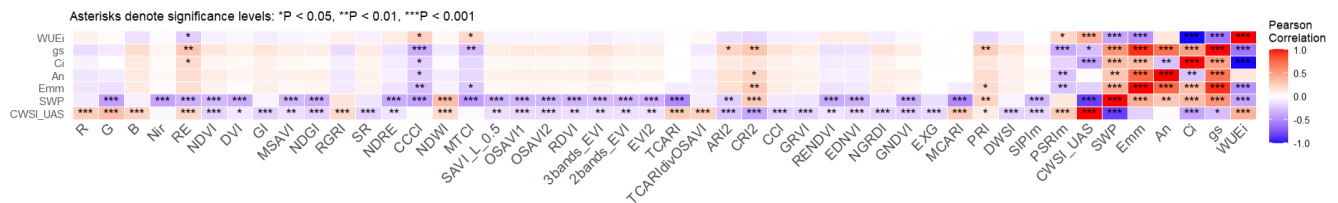

Figure 9. Pearson correlation coefficient heat map matrix of vegetative index, gas-exchange traits and CWSI. Significance levels are expressed with asterisks (*, **, *** correspond to p ≤ 0.05, 0.01 and 0.001, respectively). Positive correlations are indicated in shades of red, whereas negative correlations are indicated in shades of blue, with the intensity of the color indicating the strength of the correlation according to the scale bar at the right.

SWP shows significant negative correlations with many of the VIs and physiological traits analyzed, indicating that as water potential decreases (drier leaves), these traits tend to decrease. Some of the VIs that present strong correlations with SWP such as the transformed chlorophyll absorption in reflectance Index (TCARI), the Modified chlorophyll absorption in reflectance index (MCARI), the multispectral Structure Independent Pigment Index (SIPIm) or the Carotenoid Reflectance Index 2 (CRI2) are pigment-related indices. Some of them have been previously analyzed in other crops (Gracia-Romero et al. 2019; Katuwal et al. 2023). Despite the statistical correlation with water status found here, it seems that this relation is more related to phenological changes or senescence across growth cycle evolution than water-related physiological performance itself (Bian et al. 2019). Other indices, such as the Normalized Difference Water Index (NDWI), presented also strong correlation with SWP and CWSI_UAS as well. This result is in concordance with the study conducted by Kapari et al. (2024) denoting its applicability for water stress detection.

The other ground-based physiological variables (i.e. gs, Ci, Emm and An) showed less and weaker statistical correlations with VIs than SWP. Again, these variables were statistically correlated with pigment-related VIs such as the Clorophyll Carotenoid Index (CCI), the Canopy Chlorophyll Content Index (CCCI), the multispectral Plant Senescence Reflectance Index (PSRIm), the MERIS Terrestrial Chlorophyll Index (MTCI), the Carotenoid Reflectance Index 2 (CRI2), and the Anthocyanin Reflectance Index 2 (ARI2). Based on these results, these pigment related indices, especially those that address chlorophyll content were transversal VIs to detect variability on the ground-based physiological variables, as found in other studies (Fullana-Pericàs et al. 2022; Savchik et al. 2024). These results point these VIs as promising operative variables to monitor physiological performance in almond. However, none of the VIs performed better than CWSI_UAS to detect SWP changes (Fig. 8). In this sense, CWSI_UAS remains as a remarkable proxy for water status monitoring in almond. These relationships between certain VIs with

Proceedings of the 16th International Conference on Precision Agriculture
21-24 July, 2024, Manhattan, Kansas, United States

12

photosynthetic rates can serve as valuable tools for identifying high-performing areas in the field or detecting early signs of stress before they become apparent to the naked eye. However, it should be considered that the current study focuses on almond orchards with the same cultivar and under similar nutrient management conditions, being water status, the most changing factor affecting physiological performance. In this sense, further research is needed in almond orchard to provide feasible results on these and other VIs for almond farm management. However, this first attempt with the analyzed VIs and CWSI with ground-based physiological measurements, reinforce the operability of remote sensing technologies in enhancing water use efficiency in almond, particularly critical in water-scarce regions like southeast Spain.

Conclusion

The findings of this study illustrate that CWSI, when monitored through both ground-based and UAS-based methods, serves as a reliable tool for assessing water status in almond orchards. These results align with previous studies, reinforcing the CWSI's sensitivity in detecting water stress before it adversely affects photosynthesis, thereby proving its value for operational water status assessment. The significant correlations identified between CWSI and VIs monitored via UAS with ground-based physiological data underscore the broad applicability of this technology in almond orchard management. The use of UAS to derive CWSI highlights its practicality and effectiveness for large-scale monitoring, addressing the limitations of labor-intensive and less practical ground-based manual measurements. Additionally, integrating VIs, particularly pigment-related indices such as CCCI, MTCI, ARI2, CRI2, PRI, and PSRIm, with ground-based measurements provides a validated approach for precise physiological monitoring of almonds. The integration of CWSI maps with growth variability maps confirms that UAS-based thermal imaging is a powerful tool for monitoring crop water stress, offering high-resolution spatial variability maps crucial for precision agriculture. However, achieving reliable results in thermal monitoring, particularly with UAS, necessitates meticulous data pre-treatment and calibration. In summary, by understanding the relationships between UAS-based indices and physiological traits analyzed in this study, farmers and agronomists can improve decision-making processes related to irrigation, fertilization, and overall crop management.

Acknowledgments

References

Ahmad, U., Alvino, A., & Marino, S. (2021, October 1). A review of crop water stress assessment using remote sensing. Remote Sensing. MDPI. https://doi.org/10.3390/rs13204155

Ali, M. M., Bachik, N. A., Muhadi, N. 'Atirah, Tuan Yusof, T. N., & Gomes, C. (2019, December 1). Non-destructive techniques of detecting plant diseases: A review. Physiological and Molecular Plant Pathology. Academic Press. https://doi.org/10.1016/j.pmpp.2019.101426

Allen, R. G., Pereira, L. S., Raes, D., & Smith, M. (1998). Crop evapotranspiration-Guidelines for computing crop water requirements-FAO Irrigation and drainage paper 56.

Araus, J. L., & Cairns, J. E. (2014, January). Field high-throughput phenotyping: The new crop breeding frontier. Trends in Plant Science. https://doi.org/10.1016/j.tplants.2013.09.008

Bellvert, J., Zarco-Tejada, P. J., Girona, J., & Fereres, E. (2014). Mapping crop water stress index in a 'Pinot-noir' vineyard: Comparing ground measurements with thermal remote sensing imagery from an unmanned aerial vehicle. Precision Agriculture, 15(4), 361–376. https://doi.org/10.1007/s11119-013-9334-5

Bellvert, Joaquim, Adeline, K., Baram, S., Pierce, L., Sanden, B. L., & Smart, D. R. (2018). monitoring crop evapotranspiration and crop coefficients over an almond and pistachio orchard throughout remote sensing. Remote Sensing, 10(12). https://doi.org/10.3390/rs10122001

Bellvert, Joaquim, Marsal, J., Girona, J., Gonzalez-Dugo, V., Fereres, E., Ustin, S. L., & Zarco-Tejada, P. J. (2016). Airborne thermal imagery to detect the seasonal evolution of crop water status in peach, nectarine and Saturn peach orchards. Remote Sensing, 8(1). https://doi.org/10.3390/rs8010039

Proceedings of the 16th International Conference on Precision Agriculture
21-24 July, 2024, Manhattan, Kansas, United States

13

Berger, K., Machwitz, M., Kycko, M., Kefauver, S. C., Van Wittenberghe, S., Gerhards, M., et al. (2022, October 1). Multi-sensor spectral synergies for crop stress detection and monitoring in the optical domain: A review. Remote Sensing of Environment. Elsevier Inc. https://doi.org/10.1016/j.rse.2022.113198

Berni, J. A. J., Zarco-Tejada, P. J., Sepulcre-Cantó, G., Fereres, E., & Villalobos, F. (2009). Mapping canopy conductance and CWSI in olive orchards using high resolution thermal remote sensing imagery. Remote Sensing of Environment, 113(11), 2380–2388. https://doi.org/10.1016/j.rse.2009.06.018

Bhatti, S., Heeren, D. M., O'Shaughnessy, S. A., Neale, C. M. U., LaRue, J., Melvin, S., et al. (2023). Toward automated irrigation management with integrated crop water stress index and spatial soil water balance. Precision Agriculture, 24(6), 2223–2247. https://doi.org/10.1007/s11119-023-10038-4

Bian, J., Zhang, Z., Chen, J., Chen, H., Cui, C., Li, X., et al. (2019). Simplified evaluation of cotton water stress using high resolution unmanned aerial vehicle thermal imagery. Remote Sensing, 11(3). https://doi.org/10.3390/rs11030267

Burchard-Levine, V., Borra-Serrano, I., Peña, J. M., Kustas, W. P., Guerra, J. G., Dorado, J., et al. (2024). Evaluating the precise grapevine water stress detection using unmanned aerial vehicles and evapotranspiration-based metrics. Irrigation Science. https://doi.org/10.1007/s00271-024-00931-9

Campos, I., Neale, C. M. U., Calera, A., Balbontín, C., & González-Piqueras, J. (2010). Assessing satellite-based basal crop coefficients for irrigated grapes (Vitis vinifera L.). Agricultural Water Management, 98(1), 45–54. https://doi.org/10.1016/j.agwat.2010.07.011

Campoy, J., Campos, I., Plaza, C., Calera, M., Jiménez, N., Bodas, V., & Calera, A. (2019). Water use efficiency and light use efficiency in garlic using a remote sensing-based approach. Agricultural Water Management, 219, 40–48. https://doi.org/10.1016/j.agwat.2019.03.032

Chaves, M. M., Maroco, J. P., & Pereira, J. S. (2003). Understanding plant responses to drought - From genes to the whole plant. Functional Plant Biology. https://doi.org/10.1071/FP02076

Coll, C., Niclòs, R., Puchades, J., García-Santos, V., Galve, J. M., Pérez-Planells, L., et al. (2019). Laboratory calibration and field measurement of land surface temperature and emissivity using thermal infrared multiband radiometers. International Journal of Applied Earth Observation and Geoinformation, 78, 227–239. https://doi.org/10.1016/j.jag.2019.02.002

Costa, J. M., Egipto, R., Sánchez-Virosta, A., Lopes, C. M., & Chaves, M. M. (2019). Canopy and soil thermal patterns to support water and heat stress management in vineyards. Agricultural Water Management, 216, 484–496. https://doi.org/10.1016/j.agwat.2018.06.001

Costa, Joaquim Miguel, Marques da Silva, J., Pinheiro, C., Barón, M., Mylona, P., Centritto, M., et al. (2019, September 25). Opportunities and Limitations of Crop Phenotyping in Southern European Countries. Frontiers in Plant Science. Frontiers Media S.A. https://doi.org/10.3389/fpls.2019.01125

Fullana-Pericàs, M., Conesa, M., Gago, J., Ribas-Carbó, M., & Galmés, J. (2022). High-throughput phenotyping of a large tomato collection under water deficit: Combining UAVs' remote sensing with conventional leaf-level physiologic and agronomic measurements. Agricultural Water Management, 260. https://doi.org/10.1016/j.agwat.2021.107283

Gómez-Candón, D., Bellvert, J., & Royo, C. (2021). Performance of the Two-Source Energy Balance (TSEB) Model as a Tool for Monitoring the Response of Durum Wheat to Drought by High-Throughput Field Phenotyping. Frontiers in Plant Science, 12. https://doi.org/10.3389/fpls.2021.658357

Gómez-Candón, D., Virlet, N., Labbé, S., Jolivot, A., & Regnard, J. L. (2016). Field phenotyping of water stress at tree scale by UAV-sensed imagery: new insights for thermal acquisition and calibration. Precision Agriculture, 17(6), 786–800. https://doi.org/10.1007/s11119-016-9449-6

Gonzalez-Dugo, V., Lopez-Lopez, M., Espadafor, M., Orgaz, F., Testi, L., Zarco-Tejada, P., et al. (2019). Transpiration from canopy temperature: Implications for the assessment of crop yield in almond orchards. European Journal of Agronomy, 105, 78–85. https://doi.org/https://doi.org/10.1016/j.eja.2019.01.010

Gonzalez-Dugo, V., & Zarco-Tejada, P. J. (2024). Assessing the impact of measurement errors in the calculation of CWSI for characterizing the water status of several crop species. Irrigation Science, 42(3), 431–443. https://doi.org/10.1007/s00271-022-00819-6

Gonzalez-Dugo, V., Zarco-Tejada, P. J., & Fereres, E. (2014). Applicability and limitations of using the crop water stress index as an indicator of water deficits in citrus orchards. Agricultural and Forest Meteorology, 198–199, 94–104. https://doi.org/10.1016/j.agrformet.2014.08.003

Gracia-Romero, A., Kefauver, S. C., Fernandez-Gallego, J. A., Vergara-Díaz, O., Nieto-Taladriz, M. T., & Araus, J. L. (2019). UAV and ground image-based phenotyping: A proof of concept with durum wheat. Remote Sensing, 11(10). https://doi.org/10.3390/rs11101244

Guimarães, N., Sousa, J. J., Pádua, L., Bento, A., & Couto, P. (2024, March 1). Remote Sensing Applications in Almond Orchards: A Comprehensive Systematic Review of Current Insights, Research Gaps, and Future Prospects. Applied Sciences (Switzerland). Multidisciplinary Digital Publishing Institute (MDPI). https://doi.org/10.3390/app14051749

Gutiérrez-Gordillo, S., García-Tejero, I. F., Durán Zuazo, V. H., Escalera, A. G., Gil, F. F., Amores-Agüera, J. J., et al. (2020). Assessing the water-stress baselines by thermal imaging for irrigation management in almond plantations under water scarcity conditions. Water (Switzerland), 12(5). https://doi.org/10.3390/W12051298

Idso, S. B., Jackson, R. D., Pinter, P. J., Reginato, R. J., & Hatfield, J. L. (1981). NORMALIZING THE STRESS-DEGREE-DAY PARAMETER FOR ENVIRONMENTAL VARIABILITY*. Agricultural Meteorology (Vol. 24).

Kapari, M., Sibanda, M., Magidi, J., Mabhaudhi, T., Nhamo, L., & Mpandeli, S. (2024). Comparing Machine Learning Algorithms for Estimating the Maize Crop Water Stress Index (CWSI) Using UAV-Acquired Remotely Sensed Data

Proceedings of the 16th International Conference on Precision Agriculture
21-24 July, 2024, Manhattan, Kansas, United States

14

in Smallholder Croplands. Drones, 8(2). https://doi.org/10.3390/drones8020061

Katuwal, K. B., Yang, H., & Huang, B. (2023). Evaluation of phenotypic and photosynthetic indices to detect water stress in perennial grass species using hyperspectral, multispectral and chlorophyll fluorescence imaging. Grass Research, 3. https://doi.org/10.48130/GR-2023-0016

Legrand, M., Pietras, C., Rard Brogniez, G. É., Khalil Abuhassan, N., Michae¨, M., & Sicard, M. (2000). A High-Accuracy Multiwavelength Radiometer for In Situ Measurements in the Thermal Infrared. Part I: Characterization of the Instrument.

Martínez-Valderrama, J., Olcina, J., Delacámara, G., Guirado, E., & Maestre, F. T. (2023). Complex Policy Mixes are Needed to Cope with Agricultural Water Demands Under Climate Change. Water Resources Management, 37(6–7), 2805–2834. https://doi.org/10.1007/s11269-023-03481-5

Montoya, F., Sánchez, J. M., González-Piqueras, J., & López-Urrea, R. (2022). Is the Subsurface Drip the Most Sustainable Irrigation System for Almond Orchards in Water-Scarce Areas? Agronomy, 12(8). https://doi.org/10.3390/agronomy12081778

Morison, J. I. L., Baker, N. R., Mullineaux, P. M., & Davies, W. J. (2007). Improving water use in crop production. Philosophical Transactions of the Royal Society B: Biological Sciences, 363(1491), 639–658. https://doi.org/10.1098/rstb.2007.2175

Neupane, J., & Guo, W. (2019, February 14). Agronomic basis and strategies for precision water management: A review. Agronomy. MDPI AG. https://doi.org/10.3390/agronomy9020087

Pardo, J. J., Sánchez-Virosta, A., Léllis, B. C., Domínguez, A., & Martínez-Romero, A. (2022). Physiological basis to assess barley response to optimized regulated deficit irrigation for limited volumes of water (ORDIL). Agricultural Water Management, 274. https://doi.org/10.1016/j.agwat.2022.107917

Prueger, J. H., Parry, C. K., Kustas, W. P., Alfieri, J. G., Alsina, M. M., Nieto, H., et al. (2019). Crop Water Stress Index of an irrigated vineyard in the Central Valley of California. Irrigation Science, 37(3), 297–313. https://doi.org/10.1007/s00271-018-0598-4

Rallo, G., Paço, T. A., Paredes, P., Puig-Sirera, Massai, R., Provenzano, G., & Pereira, L. S. (2021, May 1). Updated single and dual crop coefficients for tree and vine fruit crops. Agricultural Water Management. Elsevier B.V. https://doi.org/10.1016/j.agwat.2020.106645

Ramírez-Cuesta, J. M., Ortuño, M. F., Gonzalez-Dugo, V., Zarco-Tejada, P. J., Parra, M., Rubio-Asensio, J. S., & Intrigliolo, D. S. (2022). Assessment of peach trees water status and leaf gas exchange using on-the-ground versus airborne-based thermal imagery. Agricultural Water Management, 267. https://doi.org/10.1016/j.agwat.2022.107628

Roma, E., Catania, P., Vallone, M., & Orlando, S. (2023). Unmanned aerial vehicle and proximal sensing of vegetation indices in olive tree (Olea europaea). Journal of Agricultural Engineering, 54(3). https://doi.org/10.4081/jae.2023.1536

Romero-Trigueros, C., Bayona Gambín, J. M., Nortes Tortosa, P. A., Alarcón Cabañero, J. J., & Nicolás, E. N. (2019). Determination of Crop Water Stress index by infrared thermometry in grapefruit trees irrigated with saline reclaimed water combined with deficit irrigation. Remote Sensing, 11(7). https://doi.org/10.3390/rs11070757

Sánchez, J. M., López-Urrea, R., Rubio, E., González-Piqueras, J., & Caselles, V. (2014). Assessing crop coefficients of sunflower and canola using two-source energy balance and thermal radiometry. Agricultural Water Management, 137, 23–29. https://doi.org/10.1016/j.agwat.2014.02.002

Sánchez-Piñero, M., Martín-Palomo, M. J., Andreu, L., Moriana, A., & Corell, M. (2022). Evaluation of a simplified methodology to estimate the CWSI in olive orchards. Agricultural Water Management, 269. https://doi.org/10.1016/j.agwat.2022.107729

Sánchez-Virosta, Á., & Sánchez-Gómez, D. (2020). Thermography as a tool to assess inter-cultivar variability in garlic performance along variations of soil water availability. Remote Sensing, 12(18). https://doi.org/10.3390/RS12182990

Savchik, P., Nocco, M., & Kisekka, I. (2024). Mapping almond stem water potential using machine learning and multispectral imagery. Irrigation Science. https://doi.org/10.1007/s00271-024-00932-8

Sirera, À. P., Antichi, D., Raffa, D. W., & Rallo, G. (2021). Application of remote sensing techniques to discriminate the effect of different soil management treatments over rainfed vineyards in chianti terroir. Remote Sensing, 13(4), 1–25. https://doi.org/10.3390/rs13040716

Sishodia, R. P., Ray, R. L., & Singh, S. K. (2020). Applications of remote sensing in precision agriculture: A review. Remote Sensing, 12(19), 1–31. https://doi.org/10.3390/rs12193136

Sperling, O., Gardi, I., Ben-Gal, A., & Kamai, T. (2023). Deficit irrigation limits almond trees' photosynthetic productivity and compromises yields. Agricultural Water Management, 289. https://doi.org/10.1016/j.agwat.2023.108562

Tian, X., Dong, J., Jin, S., He, H., Yin, H., & Chen, X. (2023). Climate change impacts on regional agricultural irrigation water use in semi-arid environments. Agricultural Water Management, 281. https://doi.org/10.1016/j.agwat.2023.108239

Tunca, E., Köksal, E. S., & Çetin Taner, S. (2023). Calibrating UAV thermal sensors using machine learning methods for improved accuracy in agricultural applications. Infrared Physics and Technology, 133. https://doi.org/10.1016/j.infrared.2023.104804

Zhang, L., Zhang, H., Niu, Y., & Han, W. (2019). Mapping maizewater stress based on UAV multispectral remote sensing. Remote Sensing, 11(6). https://doi.org/10.3390/rs11060605

Proceedings of the 16th International Conference on Precision Agriculture
21-24 July, 2024, Manhattan, Kansas, United States

15